7-21-93
REPRINT
E 7831

NASA Technical Memorandum 106148
AIAA–93–2521

Initial Results From the NASA-Lewis Wave Rotor Experiment

Jack Wilson
Sverdrup Technology, Inc.
Lewis Research Center Group
Brook Park, Ohio

and

Dennis Fronek
Lewis Research Center
Cleveland, Ohio

Prepared for the
29th Joint Propulsion Conference and Exhibit
cosponsored by the AIAA, SAE, ASME, and ASEE
Monterey, California, June 28–30, 1993

NASA

INITIAL RESULTS FROM THE NASA LEWIS WAVE ROTOR EXPERIMENT

Jack Wilson
Sverdrup Technology, Inc.
Lewis Research Center Group
Brook Park, Ohio 44142

and

Dennis Fronek
National Aeronautics and Space Administration
Lewis Research Center
Cleveland, Ohio 44135

Abstract

Wave rotors may play a role as topping cycles for jet engines, since by their use, the combustion temperature can be raised without increasing the turbine inlet temperature. In order to design a wave rotor for this, or any other application, knowledge of the loss mechanisms is required, and also how the design parameters affect those losses. At NASA Lewis Research Center, a three-port wave rotor experiment operating on the flow-divider cycle, has been started with the objective of determining the losses. The experimental scheme is a three-factor Box-Behnken design, with passage opening time, friction factor, and leakage gap as the factors. Variation of these factors is provided by using two rotors, of different length, two different passage widths for each rotor, and adjustable leakage gap. In the experiment, pressure transducers are mounted on the rotor, and give pressure traces as a function of rotational angle at the entrance and exit of a rotor passage. In addition, pitot rakes monitor the stagnation pressures for each port, and orifice meters measure the mass flows. The results show that leakage losses are very significant in the present experiment, but can be reduced considerably by decreasing the rotor to wall clearance spacing.

Nomenclature

a	speed of sound
B	width of a passage on the rotor
b_o,b_i,b_{ii}	constants defined in Eq. (5)
D_h	hydraulic diameter of passages
F	dimensionless friction parameter, defined in Eq. (3)
G	dimensionless leakage gap, defined in Eq. (4)
G_p	value of G evaluated at a port
G_w	value of G evaluated at a wall
H	height of a passage on the rotor
L	length of the rotor
P^o_{hi}	stagnation pressure at the high pressure outlet
P^o_{in}	stagnation pressure at the inlet
P^o_{lo}	stagnation pressure at the low pressure outlet
t	time
w	tangential velocity of the rotor at the radius of the passages
β	ratio of mass flow in high pressure port to total mass flow
γ	ratio of specific heats
δ	spacing between rotor and wall or port
$\delta_{b\ell}$	boundary layer thickness
η	efficiency
ν	kinematic viscosity
τ	dimensionless opening time, defined in Eq. (1)

Introduction

Wave rotors are devices which use unsteady waves to produce steady streams of gas which are at either higher or lower stagnation pressure than the input stream. The rotor itself has a set of axially aligned passages on its periphery. As the rotor rotates, these passages are alternately exposed to ports at differing pressures. Typically, at the exhaust, or low pressure, port, the passage contains gas at some higher pressure just before the passage rotates into juxtaposition with the port. Exposure to the low port pressure causes an expansion wave to propagate into the passage. Later in the cycle, the passage, now at lower pressure, will be opened to the inlet port, where the gas is at higher

pressure, thereby causing a shock wave to be propagated into the passage.

The exact sequence of waves will depend on the cycle employed. Several different cycles are possible, each serving a different function. Examples are three-port cycles, used as flow dividers or equalizers,[1] four-port cycles, used for superchargers,[2] topping cycles for gas turbine engines,[3] and a wave superheater wind-tunnel,[4] and five and nine port cycles, again intended for use as topping cycles.[5]

At NASA Lewis Research Center, the main interest in wave rotors is as a topping cycle for jet engines. This application is shown schematically in Fig. 1. Air from the compressor would pass to the wave rotor instead of going directly to the burner. The air is compressed in the wave rotor, and then proceeds to the burner. From the burner, the air returns to the wave rotor, where it expands, and in doing so, compresses the incoming air, and then is exhausted to the turbine. Since the expansion step inside the wave rotor drops the temperature of the air, the temperature of the air at the turbine inlet will be lower than the temperature of the air leaving the burner. Thus, for a fixed turbine inlet temperature, an engine with a wave rotor topping cycle will have a higher combustion temperature, and hence higher efficiency and also higher specific power, than the same engine without a wave rotor topping cycle.[6] Obviously, for maximum output, the efficiency of the wave rotor should be as high as possible, i.e., the losses should be minimized. In order to do this, it is necessary to know the source of the losses, and their dependance on controlling parameters. This study is aimed at assessing experimentally the magnitude of various wave rotor losses as a function of the parameters which affect them.

This will be achieved by measuring the performance of a wave rotor as various geometrical parameters (passage width, rotor length, and rotor-casing clearance) are varied. The losses are not specific to one cycle, and so any convenient cycle can be used for this study. For simplicity, the three-port flow divider cycle was chosen.

In order to make an experimental study of losses, a wave rotor has been built at NASA Lewis, operating on the three-port flow divider cycle. In this report is a brief statement of the philosophy of the experiment, a description of the experiment, and the measurements made. Finally, initial results are presented showing that reduction of the rotor to wall clearance gap leads to a large increase in performance.

Types of Losses

Although several wave rotors have been built in the past, no study of losses appears to have been reported, other than theoretical estimates by Hoerler.[7] Two major losses are the stagnation pressure loss in shock waves, and the mixing loss resulting from nonuniform velocity distributions in the output ports. These however, are readily calculable, and so can be included in any theoretical model of wave rotor performance. Less easy to calculate are the losses caused by the specific geometry of the wave rotor. These are the losses due to the finite passage opening time, friction, and leakage. These effects have been included in the one-dimensional computational fluid dynamics (CFD) model of Paxson,[8-10] but determination of the validity of the model, and evaluation of some constants requires recourse to experiment. Such an experiment will require variation of the parameters on which these losses depend. The parameters are described below.

Finite Passage Opening Time

Since the passages have a finite width, there is a finite time taken for a passage to rotate past the leading or trailing edge of a port, and become fully opened or closed. In the case of an input port, for which instantaneous opening of the passage would cause a shock wave to propagate down the passage, a finite opening time will result in a compression wave, which will steepen into a shock as it travels down the passage. The degree to which it steepens depends on the ratio of the opening time to the time taken by the wave to travel the length of the passage. Thus the relevant nondimensional parameter is

$$\tau = \frac{\text{Passage opening time}}{\text{Wave travel time}} = \frac{b}{w} \cdot \frac{a}{L} \tag{1}$$

where a is taken at some reference condition, e.g., the input stagnation value. Note that for any particular cycle, the rotor velocity w will be inversely proportional to the axial length of the passage L, and hence τ is determined mainly by the value of the passage width, B.

Friction

Accurate assessments of the effects of friction would require a calculation of the unsteady boundary layer development throughout the cycle—a monumental task. However, the thickness of the boundary layer on an accelerating flat plate is known from Rayleigh's solution as

$$\delta_{b\ell} = \sqrt{\nu t} \tag{2}$$

Substituting the time taken by a wave to travel down the passage for the time in Eq. (2), and dividing by the passage hydraulic diameter gives as a nondimensional friction factor,

$$F = \frac{\sqrt{\nu L/a}}{D_h} \tag{3}$$

Leakage

Leakage can take place from the passage to the casing if the passage is at high pressure, or from the casing to the passage if the passage is at low pressure. The result will be a "short-circuiting" from high pressure to low, leading to reduced performance. For any given passage, the area available for leakage is $2B\delta$ (the factor 2 is because leakage can occur at both top and bottom of a passage), and the area for regular flow is BH. Thus the nondimensional leakage parameter G, is the ratio of these two areas, i.e.,

$$G = \frac{2\delta}{H} \tag{4}$$

Experimental Design

From the above, it is clear that there are at least three parameters to vary in order to be able to obtain estimates of the losses due to the mechanisms involved. An efficient way to formulate an experiment to obtain empirical fits to the data when there are three or more variable parameters is the Box-Behnken scheme.[11] This scheme is illustrated for three variables in Fig. 2. Imagine a box, each side of which extends from the minimum value of the corresponding variable to the maximum value of the variable. Experimental readings are taken at the points indicated in the middle of each side, together with three replicate points at the center of the box. It is then possible to fit the results with a second-degree polynomial. For example, if the measured variable is η, and the independent variables are τ, F, and G, then the fit will be of the form

$$\eta = b_o + b_1\tau + B_2F + B_3G + b_{11}\tau^2 + b_{22}F^2 + b_{33}G^2 + b_{12}\tau F + b_{13}\tau G + b_{23}FG \tag{5}$$

where the constants b_o, b_i, and b_{ii} are determined from the experimental measurements. The replication of the center point provides an estimate of the experimental error.

This is the philosophy on which the NASA Lewis wave rotor experiment was based. A review of the literature showed that τ, F, and G had differed significantly for rotors built in the past, with insufficient data to determine which parameter is most important. Consequently, it was felt to be important to try to determine the efficiency as a function of τ, F, and G in the manner described above, so that the importance of each variable can be ascertained. In order to be able to change τ and F, the actual experiment consists of two different rotors, both 12 in. in diameter, but one 18 in. long, the other 9 in. long. Both were built with passages 0.25 in. wide, and 0.4 in. high, with 120 passages per rotor. After a series of runs at 0.25 in. passage width, every other wall will be removed, and another series run at approximately twice the passage width. This combination gives three values of τ, and three values of F.

Leakage between the rotor and the casing will occur predominantly where the pressure difference between the casing and rotor passage is large. Initially, it was thought that this would be only at the high and low pressure ports, and that therefore it would only be necessary to vary the leakage parameter G at the ports. In order to do this, the ports were built as inserts. Placing shims under the flange of the insert permits variation of the rotor to port gap. Later, computational results showed that a large pressure differential exists where the expansion wave reflects from the wall on the input side, and that it was necessary to control the rotor to wall gap also. A photograph of the apparatus, with the 18-in. rotor in place, is shown in Fig. 3.

As mentioned previously, wave rotors can be operated on a variety of cycles, depending on the intended purpose of the wave rotor. For an experiment of the kind envisioned here, a simple cycle, without the complications of a burner, seemed more desirable, and the three-port, flow divider cycle was selected. In prior work, it has frequently been assumed that all the waves are weak, so that the acoustic approximation can be applied. This however limits the pressure ratio to small values. For topping cycle application, the pressure ratio should be as large as possible, and so a secondary objective was to operate the wave rotor under conditions for which the acoustic approximation would not be valid.

Consequently, an expansion ratio of 0.33 was chosen, corresponding to a Mach number of the expanded flow of 0.85. The expansion ratio is the ratio of the pressure in the low pressure port to the pressure in a rotor passage just before it is opened to the low pressure port. This ratio determines the Mach number of the flow in the low pressure port.

The choice of a strong expansion meant that the cycle could not be calculated with the acoustic approximation, and either characteristics, or a CFD approach had to be used. An x-t diagram of the cycle, calculated using characteristics, assuming inviscid flow, and instantaneous port openings, is given in Fig. 4. It is assumed that the gas is at rest at uniform pressure just before it is rotated to open to the low pressure port. When the right-hand end of the passage is exposed to the low pressure port, an expansion wave travels to the left into the passage, accelerating the gas out of the passage, and into the port. As can be seen, the expansion broadens considerably as it propagates. The expansion wave reflects from the closed left-hand end of the passage, and returns to the low pressure port, slowing, and eventually stopping the outflow. When the gas velocity becomes zero, the port is closed. There are still waves inside the passage, and one of these, a compression wave generated by the reflection at the constant pressure outlet of the reflected expansion wave, gradually steepens to form a shock wave. Later, the passage rotates so that the left-hand end is exposed to the inlet port. The pressure in the passage is lower than that in the inlet port, and a shock wave is driven down the passage. The timing has been chosen so that this main shock catches up with the reflected, steepened compression wave as both reach the right-hand wall. The combined shock is now reflected off the right-hand wall, just as the high pressure port is opened. This reflected shock travels back to the left, raising the pressure, and reducing the velocity of the gas as it does so. When the shock arrives at the left-hand end, the passage rotates past the end of the input port, closing that end. Since the gas is moving to the right, this causes a small expansion wave to travel to the right, to bring the gas to rest. When this expansion reaches the right-hand end, the passage is rotating past the end of the high pressure port, closing that end, and trapping the gas inside the passage, ready to start the cycle all over again.

Experimental Measurements

Kentfield[1] has shown that the efficiency of a flow divider can be expressed as

$$\eta = \frac{\beta}{(1-\beta)} \frac{\left(P^{\circ}_{hi}/P^{\circ}_{in}\right)^{(\gamma-1)/\gamma} - 1}{1 - \left(P^{\circ}_{lo}/P^{\circ}_{in}\right)^{(\gamma-1)/\gamma}} \qquad (6)$$

Thus it is important to measure the mass flows, and the stagnation pressures of the inlet, high pressure, and low pressure flows. A schematic diagram of the apparatus is given in Fig. 5, showing how this is done. The mass flows are measured with standard orifice meters, one in each flow leg. The inlet and outlet ports are obviously sections of an annulus. A transition piece in front of the inlet port takes the flow in the inlet pipe, and converts it to the port shape, accelerating the flow in the process, as well as bringing it onto the rotor at the correct angle. Immediately upstream of the transition piece, but downstream from the orifice, is a diagnostic spool, with three wall static taps, and five pitot tubes, and a thermocouple to measure the velocity distribution at the spool. From these measurements, the mass flow, and the effective inlet stagnation pressure can be evaluated. Similarly, the output ports have transition pieces to take the flow from the port shape back to round, and which also act as diffusers. The downstream area of these diffusers is fixed by the exhaust pipe diameter. With the diffuser area ratio determined, the length was chosen to give maximum diffuser efficiency using the diffuser performance curves of Ref. 12. Initially, a diagnostic spool was placed immediately at the exit of each diffuser, but the velocity distribution was found to be very nonuniform. To cure this problem, VORTAB™ flow conditioners[13] were installed between the exit of the diffusers and the diagnostic spools. The flow conditioner pressure drop was calibrated in a separate test.

In addition to the above measurements, there were five static pressure taps on the top and bottom of each port, and four pitot tube installations. The pitot installations carried either a rake of five pitot tubes to determine radial velocity distribution, or a five-probe directional pitot probe,[14] to determine centerline velocity and direction. All steady state pressure measurements were recorded through an electronically scanned pressure (ESP) measurement system. The pressure measuring system automatically self-calibrates every 20 min. to maintain a 0.1 percent accuracy. The ESP system communicates through an Institute of Electrical and Electronics Engineers 488 interface to a state-of-the-art, real-time data acquisition system designed at NASA Lewis.[15] The data system was designed for small to medium sized aeronautics facilities, most of which are currently testing rotating machinery. The system

acquires data, converts it to engineering units, computes test dependant performance calculations, and displays the information in alphanumeric or graphical form. The cycle time is 1 sec.

Another important measurement was the dynamic on-board rotor pressure. Six dynamic pressure transducers (Endevco Model 8530, with 100 kHz response) were fitted into the rotor. Two were near the entrance to the passages, two in the center, and two near the exit. One set (entrance, center, exit) was in one passage, the other set in a passage diametrically opposed to the first set. The transducers were mounted flush with the lower wall of the passage. The signals from the transducers were taken off the rotor through a slip ring, displayed on a Tektronix oscilloscope, and recorded on tape. These measurements were used for comparisons of the actual pressure history with that calculated for the postulated cycle.

Control of the wave rotor flows was by a butterfly valve in each leg. The supply pressure was around 55 psia. The inlet valve was adjusted to throttle this supply pressure down to the desired inlet stagnation pressure, usually 30 psia. The expansion ratio was set by the low pressure valve, based on a low pressure port static pressure reading, and a pressure tap in the endwall giving the passage pressure just before opening to the low pressure port. The high pressure valve controlled the mass ratio β, based on the input and high pressure orifice mass flow readings. The rotor was turned by a variable speed electric motor with a constant speed control. An independent measurement of the rotor speed was also made.

Results

An oscillogram of the inlet and exit on-board pressure transducer signals obtained in an early run is shown in Fig. 6. The inlet signal shows that the pressure is reasonably uniform before the arrival of the expansion wave caused by the opening of the low pressure port. When the wave arrives, the pressure drops, falling to a value below that of the low pressure port. Opening of the inlet port causes the main shock to be propagated into the passage. Arrival of the reflected shock is seen briefly before the inlet port closes, creating the second expansion which brings the flow to rest. On the exit side, the pressure is constant prior to the opening of the low pressure port, then drops to the port value. Later, the high pressure port opens at the same time as the main shock is reflected, raising the pressure above the inlet pressure. The pressure falls again when the port closes simultaneously with the arrival of the second expansion. This is apparently in agreement with the postulated cycle as shown in Fig. 3; the features found in the oscillogram can be seen in Fig. 3 at a given pressure tap location by starting at $t = 0$, and moving vertically upward in the diagram. There is one exception however; in the postulated cycle, the pressure on the exit side is constant while the low pressure port is open, then falls as the tail of the reflected expansion arrives, only rising again when the main shock arrives. In the experiment, when the low pressure port is closed, a shock wave is generated, raising the pressure. The reason for this shock is seen in Fig. 7, which gives the measured velocity as a function of position in the low pressure port. Also drawn in Fig. 7 is the velocity distribution expected from the characteristics solution. The predicted velocity falls to zero at port closing, whereas the actual velocity clearly does not. Closing the passage when it still has an outward velocity will generate a hammer shock bringing the gas to rest. CFD calculations[10] were made to try to explain why the gas still had a significant outward velocity at port closing in the experiment, but not in the theory. The only losses in the characteristics calculation are mixing losses in the ducts external to the wave rotor. The CFD calculation does have finite opening, friction, and port gap leakage losses. Even when these losses were set at higher values than expected, it was not possible to create the hammer shock at the port closing. However, when endwall leakage was included, the hammer shock did appear. This is explained as follows: when the expansion wave reaches the wall at the inlet side, the pressure in the passages drops rapidly, falling below the value in the rotor casing, and thus ingesting air into the passages from the casing through the rotor-wall gap. This sets up a outward velocity in the passages which is not cancelled by the reflected expansion wave. Consequently, there is still velocity in the passages when the port closes, giving rise to the hammer shock. The magnitude of this leakage is a function of the rotor-wall gap, and this gap plays a larger role than the gap at the ports.

The conclusion above led to a redesign of the experiment to include false end-walls permitting variation of the rotor-wall gap G_w everywhere, independently of the variation of the gap at the ports G_p. An oscillogram from a run with the false walls in place is shown in Fig. 8. For this run, the value of both G_p and G_w was 0.025, compared with about 0.1 for the run of Fig. 6. It is seen that the strength of the hammer shock created by closing the low pressure port is significantly reduced. The signal from the central pressure transducer shows all the features expected from the characteristics diagram—the main expansion, the combined hammer shock and steepened compression wave, the main shock, followed by the reflected shock, and finally the secondary expansion. Thus the reduction in the leakage has resulted in a cycle very close to the postulated cycle.

The leakage reduction also gave improved performance. The performance of a flow divider can be indicated by plotting P^o_{hi}/P^o_{in} versus P^o_{lo}/P^o_{in} at a constant value of β.[1] The results of the present experiment, plotted in this manner, are shown in Fig. 9, for three values of G, namely 0.1, 0.05, and 0.025, and a nominal value of $\beta = 0.37$. As can be seen from Eq. (6), at a fixed value of β, and for a given value of P^o_{lo}/P^o_{in}, a higher P^o_{hi}/P^o_{in} corresponds to a higher efficiency. The improvement created by reducing the value of G is evident. Quantitatively,for $\beta = 0.37$, the maximum efficiency, at an expansion ratio of 0.6 (expansion Mach number = 0.38) was 0.09 for G = 0.1, whereas for G = 0.025, the maximum efficiency was 0.17 at an expansion ratio of 0.6. Using the CFD program of Paxson,[8,9] the calculated efficiency is 0.21 for $\beta = 0.37$, G = 0, and an expansion ratio of 0.6. Reducing the value of G to 0.025 has significantly improved the performance over that obtained at G = 0.1, but still further reductions in G are desirable for the performance to approach that calculated for G = 0.

Conclusions

Initial results from the NASA Lewis wave rotor experiment have demonstrated the importance of minimizing leakage between the rotor and the casing. Using a three-port, flow divider cycle, leakage was varied by adjusting the clearance gap between moveable end walls and the rotor. Reducing the clearance from 0.020 to 0.005 in. resulted in an increase in efficiency from 9 to 17 percent, for runs for which the high pressure mass flow was 0.37 times the total mass flow, and the low pressure output Mach number was 0.38. For this case, the calculated efficiency without leakage is 21 percent. The effect of leakage on the wave cycle was also observed, with the wave pattern approaching that calculated assuming no leakage as the clearance gap was reduced. Future runs will permit evaluation of the effects of friction and finite opening time as well as leakage.

References

1. Kentfield, J.A.C., "The Performance of Pressure Exchange Dividers and Equalizers," Journal of Basic Engineering, Vol. 91, Sept. 1969, pp. 361–369.

2. Jenny, E., and Zumstein, B., "Pressure Wave Supercharging of Passenger Car Diesel Engines," IMechE Conference Proceedings, Publication C44/82, The Institution of Mechanical Engineers, London, England, Apr. 1982, pp. 129–141.

3. Meyer, A., "Recent Developments in Gas Turbines," Mechanical Engineering, Vol. 69, No. 4, 1947, pp. 273–277.

4. Weatherstone, R.C., Smith, W.E., Russo, A.L., and Marrone, P.V., "Gasdynamics of a Wave Superheater Facility for Hypersonic Research and Development," Report No. AD–118–A–1, Cornell Aeronautical Laboratory, Buffalo, NY, 1959.

5. Thayer III, W.J., Taussig, R.T., Zumdieck, J.F., Vaidyanathan, T.S., and Christiansen, W.C., "Energy Exchanger Performance and Power Cycle Evaluation: Experiments and Analysis," Final Report to the Department of Energy under Contract AC06–78ER01084, Mathematical Sciences North West, Seattle, WA, Apr. 1981.

6. Wilson, J., and Paxson, D.E., "Jet Engine Performance Enhancements Through Use of a Wave Rotor Topping Cycle," To be published as NASA TM, 1993.

7. Hoerler, H.U., "Abschaetzung der Verluste in Instationaer-Gasdynamischen Kanaltrommel-Drucktauschern," Doctoral Dissertation Number 4402, Eidgenoessische Technische Hochschule, Zurich, Switzerland, 1969.

8. Paxson, D.E., "A General Numerical Model for Wave Rotor Analysis," NASA TM–105740, 1992.

9. Paxson, D.E., and Wilson, J., "An Improved Numerical Modelling Program for Wave Rotor Analysis," AIAA Paper 93-0482, 1993. (Also NASA TM–105915, 1992.)

10. Paxson, D.E., "A Comparison Between Numerically Modelled and Experimentally Measured Loss Mechanisms in Wave Rotors," AIAA Paper 93–2522, 1993.

11. Box, G.E.P., and Behnken, D.W., "Some New Three-Level Designs for the Study of Quantitative Variables," Technometrics, Vol. 2, 1960, pp. 455–475.

12. Mattingly, J.D., Heiser, W.H., and Daley, D.H., Aircraft Engine Design, AIAA Education Series, American Institute of Aeronautics and Astronautics, Washington, DC, 1987.

13. VORTAB™ Flow Conditioners are produced by Vortab Corporation, 619 Palisade Ave., Englewood Cliffs, NJ 07632.

14. Glawe, G.E., and Krause, L.N., "Miniature Probes For Use in Gas Turbine Testing," NASA TM X-71638, 1974.

15. Fronek, D.L., Setter, R.N., Blumenthal, P.Z., and Smalley, R.R., "A Distributed Data Acquisition System for Aeronautics Test Facilities," NASA TM–88961, 1987.

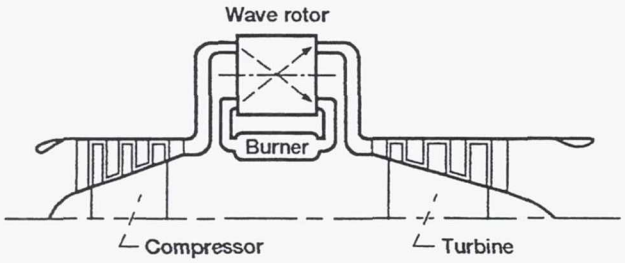

Figure 1.—Schematic diagram showing a wave rotor as a topping cycle for a jet engine.

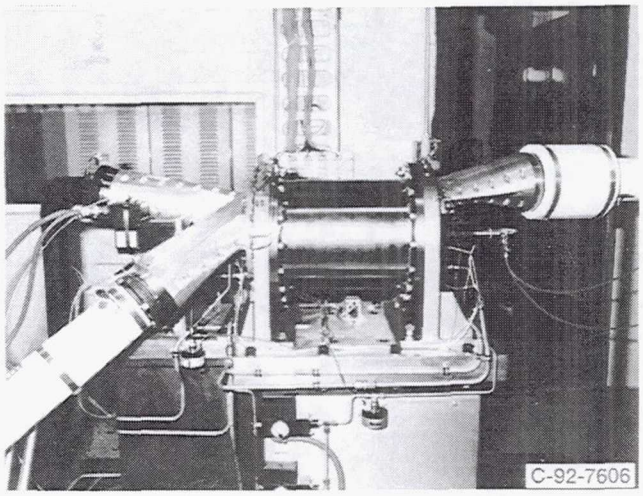

Figure 3.—Photograph of the apparatus.

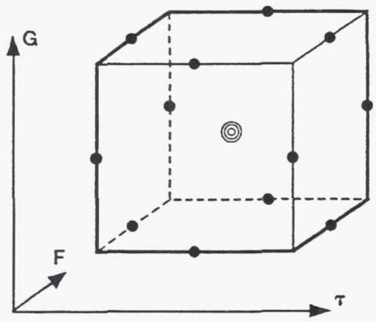

Figure 2.—Illustration of the Box-Behnken design of an experiment for three variables. Runs are made at values of the variables corresponding to the solid circles shown. In addition the center point, indicated by the three concentric circles is repeated three times.

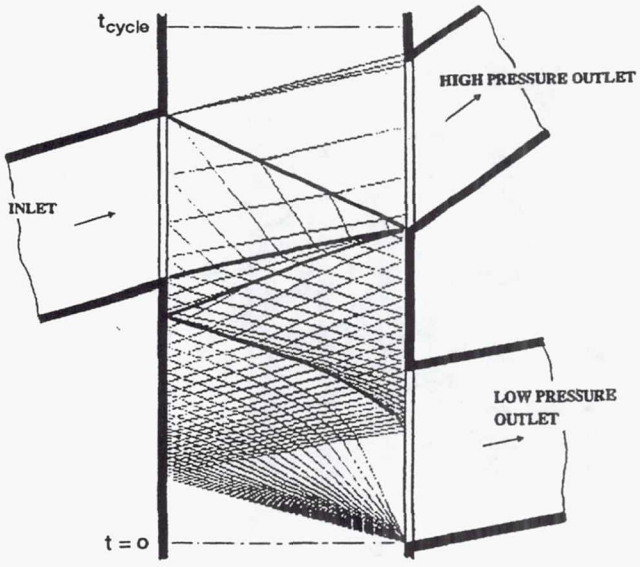

Figure 4.—An x-t diagram of the flow divider cycle chosen for the experiment, as evaluated by the method of characteristics.

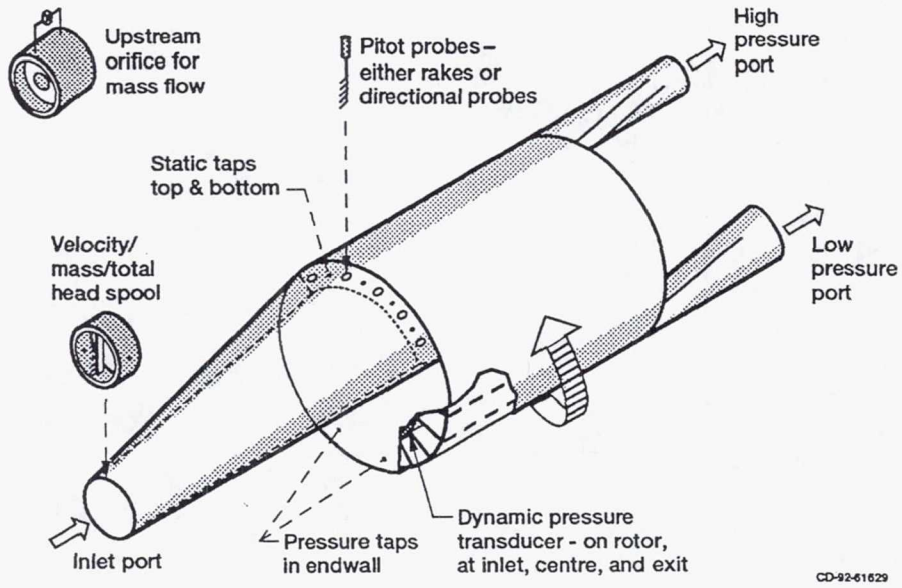

Figure 5.—Schematic diagram of the experiment, showing the diagnostics used.

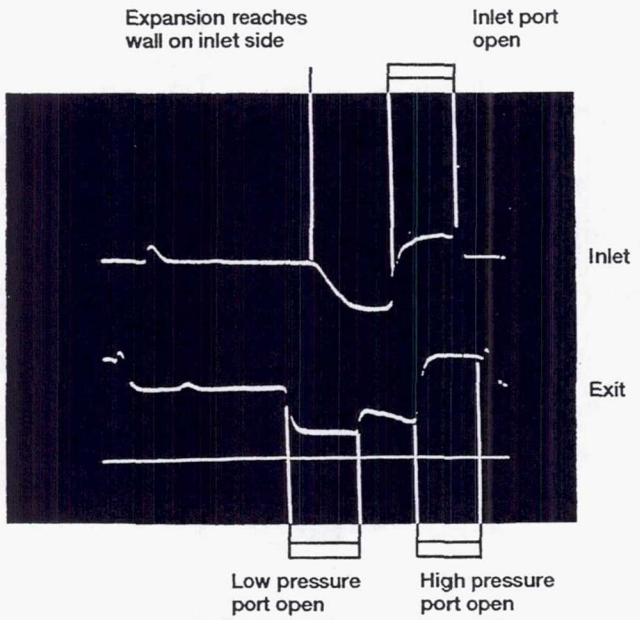

Figure 6.—Oscillogram of the trace from the on-board pressure transducers at the entrance and exit of the rotor passage in an *early run*. G = 0.1.

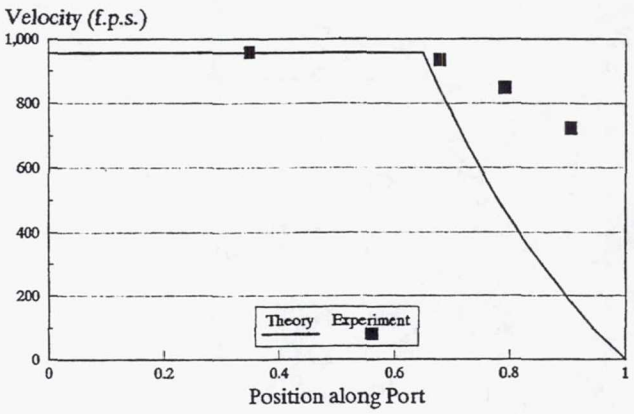

Figure 7.—Velocity as a function of position in the port for an early run, together with the predicted velocity distribution from the characteristics calculation. G = 0.1 for the experimental points.

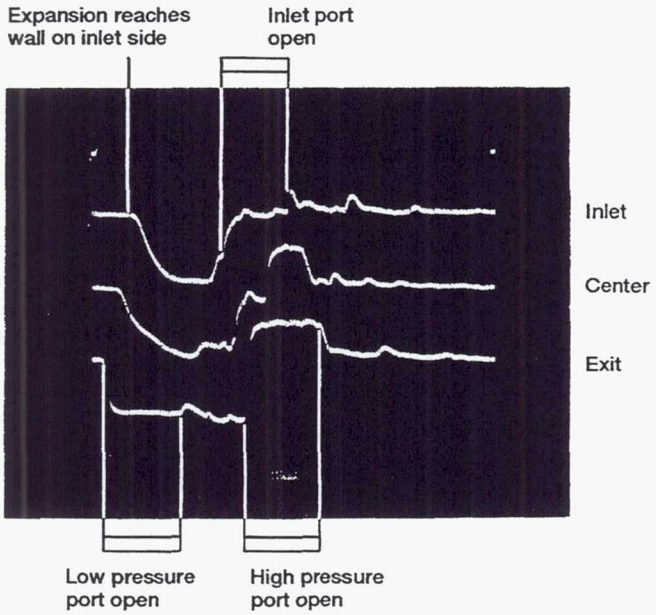

Figure 8.—Oscillogram of the trace from the on-board pressure transducers at the entrance and exit of the rotor passage in a later run with variable rotor-wall gap. G = 0.025.

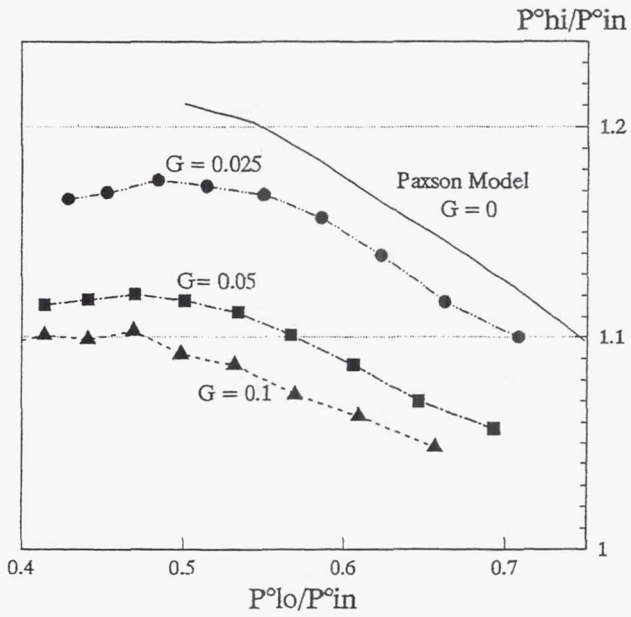

Figure 9.—Plot of flow divider performance.

REPORT DOCUMENTATION PAGE

Form Approved
OMB No. 0704-0188

1. AGENCY USE ONLY (*Leave blank*)	2. REPORT DATE	3. REPORT TYPE AND DATES COVERED
	May 1993	Technical Memorandum

4. TITLE AND SUBTITLE

Initial Results From the NASA-Lewis Wave Rotor Experiment

5. FUNDING NUMBERS

WU–505–62–10

6. AUTHOR(S)

Jack Wilson and Dennis Fronek

7. PERFORMING ORGANIZATION NAME(S) AND ADDRESS(ES)

National Aeronautics and Space Administration
Lewis Research Center
Cleveland, Ohio 44135–3191

8. PERFORMING ORGANIZATION REPORT NUMBER

E–7831

9. SPONSORING/MONITORING AGENCY NAME(S) AND ADDRESS(ES)

National Aeronautics and Space Administration
Washington, D.C. 20546–0001

10. SPONSORING/MONITORING AGENCY REPORT NUMBER

NASA TM–106148
AIAA–93–2521

11. SUPPLEMENTARY NOTES

Prepared for the AIAA, SAE, ASME, and ASEE 29th Joint Propulsion Conference and Exhibit sponsored by the American Institute of Aeronautics and Astronautics, Monterey, California, June 28–July 1, 1993. Jack Wilson, Sverdrup Technology, Inc., Lewis Research Center Group, 2001 Aerospace Parkway, Brook Park, Ohio 44142, and Dennis Fronek, NASA Lewis Research Center, Cleveland, Ohio. Responsible person, Lawrence J. Bober, (216) 433–3944.

12a. DISTRIBUTION/AVAILABILITY STATEMENT

Unclassified - Unlimited
Subject Category 07

12b. DISTRIBUTION CODE

13. ABSTRACT ***(Maximum 200 words)***

Wave rotors may play a role as topping cycles for jet engines, since by their use, the combustion temperature can be raised without increasing the turbine inlet temperature. In order to design a wave rotor for this, or any other application, knowledge of the loss mechanisms is required, and also how the design parameters affect those losses. At NASA Lewis Research Center, a 3-port wave rotor experiment operating on the flow-divider cycle, has been started with the objective of determining the losses. The experimental scheme is a three factor Box-Behnken design, with passage opening time, friction factor, and leakage gap as the factors. Variation of these factors is provided by using two rotors, of different length, two different passage widths for each rotor, and adjustable leakage gap. In the experiment, pressure transducers are mounted on the rotor, and give pressure traces as a function of rotational angle at the entrance and exit of a rotor passage. In addition, pitot rakes monitor the stagnation pressures for each port, and orifice meters measure the mass flows. The results show that leakage losses are very significant in the present experiment, but can be reduced considerably by decreasing the rotor to wall clearance spacing.

14. SUBJECT TERMS	15. NUMBER OF PAGES
Wave rotor; Topping cylce; Jet engine; Flow divider cycle	10
	16. PRICE CODE A02

17. SECURITY CLASSIFICATION OF REPORT	18. SECURITY CLASSIFICATION OF THIS PAGE	19. SECURITY CLASSIFICATION OF ABSTRACT	20. LIMITATION OF ABSTRACT
Unclassified	Unclassified	Unclassified	